



Coupled heat conduction and multiphase change problem accounting for thermal contact resistance

Daniel Weisz-Patrault

► To cite this version:

Daniel Weisz-Patrault. Coupled heat conduction and multiphase change problem accounting for thermal contact resistance. International Journal of Heat and Mass Transfer, 2017, 104, pp.595-606. 10.1016/j.ijheatmasstransfer.2016.08.091 . hal-01365342

HAL Id: hal-01365342

<https://hal.science/hal-01365342>

Submitted on 13 Sep 2016

HAL is a multi-disciplinary open access archive for the deposit and dissemination of scientific research documents, whether they are published or not. The documents may come from teaching and research institutions in France or abroad, or from public or private research centers.

L'archive ouverte pluridisciplinaire **HAL**, est destinée au dépôt et à la diffusion de documents scientifiques de niveau recherche, publiés ou non, émanant des établissements d'enseignement et de recherche français ou étrangers, des laboratoires publics ou privés.

Coupled heat conduction and multiphase change problem accounting for thermal contact resistance

Daniel Weisz-Patrault

LMS, École Polytechnique, CNRS, Université Paris-Saclay, 91128 Palaiseau, France

Abstract

In this paper, heat conduction coupled with multiphase changes are considered in a cylindrical multilayer composite accounting for thermal contact resistance depending on contact pressures and roughness parameters. A numerical simulation is proposed using both analytical developments and numerical computations. The presented modeling strategy relies on an algorithm that alternates between heat conduction accounting for volumetric heat sources and a multiphase change model based on non-isothermal Avrami's equation using the isokinetic assumption. Applications to coiling process (winding of a steel strip on itself) are considered. Indeed, phase changes determine the microstructure of the final material and are responsible for residual stresses that create flatness defects. A Finite Element modeling is used for validating the presented solution and numerical results are presented and discussed.

Keywords: Multiphase changes, Heat conduction, Analytical solution, Coiling process

1. Introduction

1.1. Heat conduction problem in a multilayer composite

A cylindrical multilayer composite is considered as shown in figure 1a. Contact pressures, that can vanish if contact is not ensured, are known as well as heterogeneous initial temperature and phase fields. This paper aims at developing a modeling strategy enabling effective simulation of the unsteady heat conduction problem, accounting for multiphase changes that occur during cooling. Since applications to axisymmetric coil cooling problems are considered, a radial model is derived, although the circumferential direction could have been addressed. Heat fluxes along the axial direction are neglected despite the fact that the temperature field slightly evolves along the axial direction because of contact pressure distribution and boundary conditions at cylinder edges. Therefore, a one-dimensional problem is obtained and applied several times at different axial locations. Industrial temperature measurements, recorded with an infrared camera during coil cooling, are presented in figure 1b. The axisymmetric assumption is well verified.

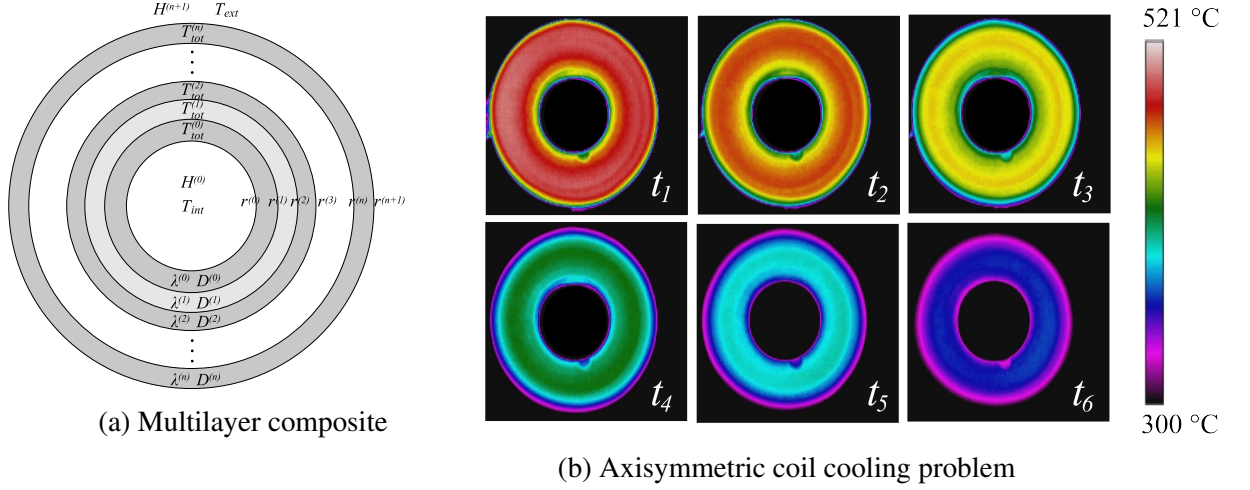


Figure 1: Heat conduction modeling

The heat conduction modeling strategy relies on analytical developments. This choice leads to reasonable computation times that enable parametric studies. Analytical solutions for multilayer composites have already been studied. For instance, the analytical solution of the unsteady heat conduction problem without heat sources in a 1D multilayer composite has been established in plates, cylinders and spheres by De Monte [1, 2]. An extension has been proposed by De Monte [3] for a 2D bi-layer composite in Cartesian coordinates. More recently Singh et al. [4], Jain et al. [5] extended this solution for a cylindrical 2D multilayer composite (radial and circumferential directions) considering time-independent heat sources. The same problem has been solved for spherical configurations by Jain et al. [6]. The radial 1D heat conduction problem for a bi-layer composite has been recently solved by Li and Lai [7] using Laplace transforms. All these works do not consider heat sources or deal with time-independent heat sources. In this paper, a coupling with multiphase change problems is considered, thus time and space dependent heat sources should be taken into account.

Necati Özışık [8] obtained a very elegant solution for the 1D heat conduction problem in multilayer composites (plate, cylinder and sphere) considering time and space dependent heat sources. A compact closed-form solution, very suitable for analytical heat sources, is proposed. However, in this paper heat sources are given numerically as outputs of the multiphase change problem, with a given time and space discretization. It should be noted that a direct numerical computation of the closed-form solution proposed in [8] would not be efficient in terms of computation times. Indeed, the latter solution relies for each time t on a primitive denoted by $\int_0^t g_n^*(t') dt'$, where functions $g_n^*(t')$ are defined for each time t' as a sum of several numerical integrals over the strip thickness. The time discretization can be very fine, so that phase changes are correctly described. Since t' lies between 0 and t the time discretization for the integrand $g_n^*(t')$ should be even finer and numerical evaluations of the proposed solution are long for the considered applications. The solution presented in [8] relies on an expansion of heat sources into a series of the form (25). In this paper, an alternative idea is to expand heat sources into time-dependent exponential series by using data fit procedures. The obtained solution avoids long numerical computations of $g_n^*(t')$ and mainly rely on matrix inversion. One could have used the closed-form solution in [8] at this point, however calculations are done under the assumption that heat fluxes vanish at the inner radius. The solution could be fairly easily

adapted for a surrounding temperature at the inner radius identical to those at the outer radius, but more significant changes should be made if the surrounding temperature at the inner radius is different from those at the outer radius. Therefore, the analytical solution derived in the following enables to consider different surrounding temperatures at inner and outer surfaces. Mathematical developments rely on quite similar ideas developed in [8] on the one hand and data fit procedures on the other hand.

1.2. Thermal contact resistance

Furthermore, contact pressures between layers are assumed to be known. Therefore, thermal contact resistance can be evaluated depending on roughness profiles. All previously cited analytical solutions deal with continuous temperature and heat flux through each interface, which corresponds to perfect thermal contact. Indeed, orthogonality relations that are used to fulfill the initial condition do not hold if thermal contact resistances are introduced. In this paper, this difficulty is overcome by assuming perfect contact conditions, however thin insulating air gaps between steel layers are introduced, in order to model an equivalent thermal contact resistance. The appropriate air gap thickness is determined as a function of thermal contact resistance by ensuring that the heat flux flowing through the imperfect interface is the same as the average heat flux flowing through the equivalent air gap. The macroscopic temperature discontinuity at the interface that defines thermal contact resistance is presented in principle in figure 2a. The modeling strategy relying on temperature and flux continuities, thin insulating air gaps are introduced in order to smooth interface discontinuities without pretending a better description of the real contact. Indeed, the latter smoothing is rather artificial and relies completely on established thermal contact resistance that characterizes stochastic properties of real contact topology.

Determination of thermal contact resistance between rough surfaces has been intensively studied. Kaza [9] presents an interesting review of the field and based on contact theories and experiments a thermal contact resistance that depends on roughness parameters and contact pressure is proposed. This latter thermal contact resistance is used in this paper. The real contact area is only a small proportion of the nominal contact area according to roughness of both surfaces. There remain asperities that are filled usually with a gas or a liquid if contact is lubricated. Early papers of Shlykov and Ganin [10] and Cooper et al. [11] describe a calculation method of thermal contact resistance for steel, depending on contact pressure and roughness. Two thermal contact resistances considered as parallel resistances are identified, namely constriction resistance and resistance of asperities. On the one hand, constriction resistance describes the fact that the heat flux narrows towards the actual contact spots. On the other hand, resistance of asperities represents the insulation due to the fluid that lies in the asperities. These classical contributions are represented in figure 2b. Models based on stochastic treatments of asperities have been developed by Mikić [12, 13] and take the interface deformation into account. For lubricated contacts one can mention more recent models developed by Hamasaiid et al. [14] and Yuan et al. [15] giving analytical predictions of thermal contact resistance at liquid-solid interfaces. Most models have been validated experimentally for low contact pressures, Fieberg and Kneer [16] proposed an experimental setup in order to measure thermal contact resistance under higher pressure and temperature conditions.

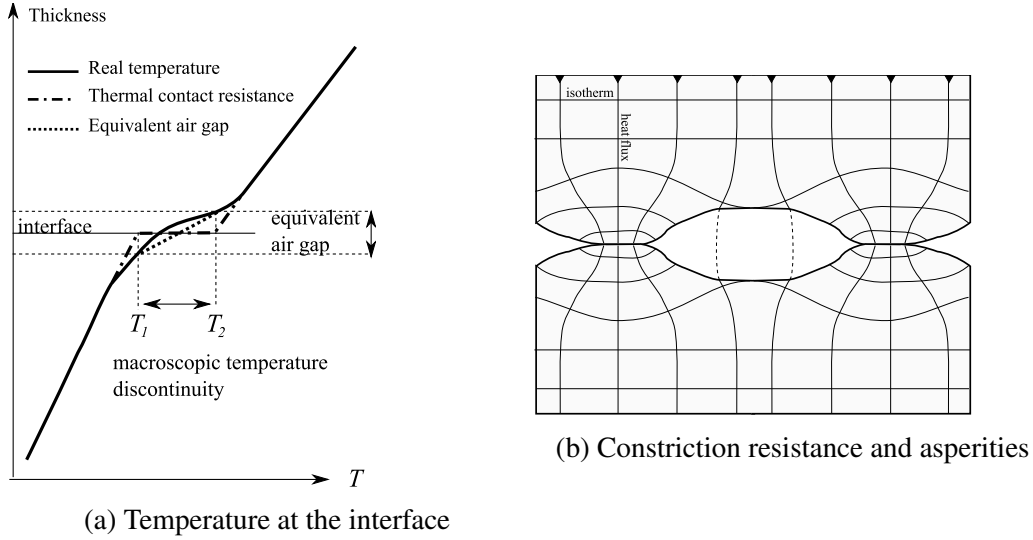


Figure 2: Thermal contact resistance

1.3. Multiphase change

In this paper, phase changes that occur during cooling are considered. Solid iron has only two possible phases, namely austenite or (γ) phase that is stable at high temperature and corresponds to a face-centered cubic lattice (fcc) and ferrite or (α) phase that is stable at room temperature and corresponds to a body-centered cubic lattice (bcc). Steel being an alloy of iron and carbon (and other chemical additives such as manganese, chlorine etc...) more complicated patterns can be formed. A schematic phase diagram Fe-C is presented in figure 3. Several configurations are therefore identified as different steel phases such as austenite, ferrite, pearlite, bainite and martensite. Schematically during cooling, austenite is transformed into ferrite. Carbon solubility in ferrite being very small, carbon atoms migrate towards austenite and carbon concentration increases. When austenite is saturated in carbon atoms, the latter precipitate and form cementite (Fe_3C). Thus, pearlite then bainite are formed, depending on geometrical patterns between ferrite and cementite. If a characteristic temperature MS is reached, martensite can be produced from residual austenite. It basically consists in a fast transformation without carbon migration. All these phases are considered in the following, however this paper does not focus on their metallurgical or mechanical aspects. The different stages through which a phase change occur are classically nucleation, growth and coalescence. A review of this field is given for instance by Pan [17]. In this paper, only the overall kinetics of the phase transformation, giving the transformation rate, is needed. Avrami [18] gives the well-known fundamental equation (31) predicting transformation kinetics for diffusive transformations under isothermal assumption. The solution is based on the idea that small germ nuclei of the new phase are pre-existing and can be transformed into active growth nuclei or be swallowed by growing grains of the new phase. Statistical treatments are used to compute the overlapping volume between different growing grains. Avrami [18] also defines the isokinetic range as the assumption that the growth rate is proportional to the probability of creating active growth nuclei from germ nuclei. For non-isothermal conditions, the isokinetic assumption has been extended by Cahn [19] leading to equation (32) as reviewed for instance by Christian [20]. On the other hand, the diffusionless martensite transformation is modeled using the work of Koistinen and Marburger [21]. The purpose of this paper is not to develop an original multiphase transformation model,

the main issue being to propose an efficient modeling strategy to couple heat conduction and multiphase change problems.

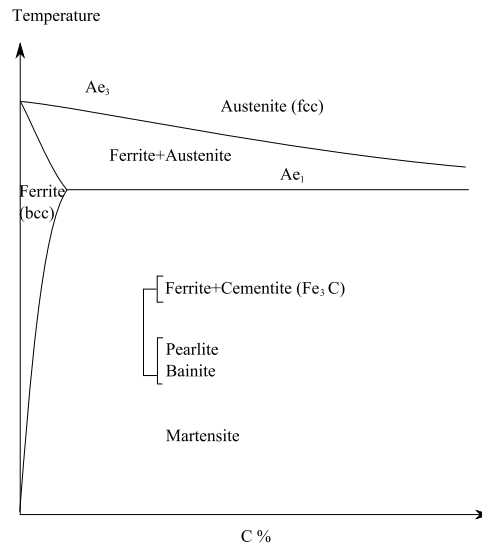


Figure 3: Phase diagram Fe-C

1.4. Applications

Applications to coiling process are considered. This consists in winding under tension a steel strip on a cylindrical mandrel. This process is very commonly used in the steel making industry for storage. Residual stress issues are significant during coiling process. Indeed, plastic deformations and phase changes occur during the winding of the strip on itself. Based on previous works [22, 23], a mechanical model has been recently proposed by Weisz-Patrault et al. [24] in order to solve (with reasonable computation times) this highly nonlinear problem, where rough contacts of the strip on itself, elastic-plastic behavior and large rotations are involved. The final residual stress profile is one of the main outputs. One can extract from this latter model both geometry and contact pressures in the coil that are assumed to be known in the present paper. Phase changes aspects during the coil cooling are also significant with respect to residual stress issues. Indeed, when the final coil stored in order to cool down, phase changes occur modifying the residual stress profile. A very few attempts to a better understanding of this part of the process have been published. For instance Park et al. [25], Saboonchi and Hassanpour [26], Karlberg [27] proposed numerical models dedicated to the heat conduction problem in the coil without phase transformation. A coupling with thermal and phase change problems is proposed for coil annealing by Mehta and Sahay [28].

1.5. Organization of the paper

The paper is organized as follows. In section 2 heat conduction is solved analytically, in a cylindrical multilayer composite accounting for known time-dependent heat sources. Suitable series expansion is proposed for heat sources, so that an analytical particular solution can be found. Multiphase changes are addressed in section 3, assuming a known temperature field. A summary of the coupling algorithm is given in section 4. In section 5, a brief and simple model enables to fix air gaps thicknesses in order to take into account thermal contact resistance.

In section 6, a Finite Element model is carried out, in order to validate the exactness of the proposed solution. Eventually, the model is tested and results are discussed in section 7.

2. Heat conduction problem

Assuming multiphase changes, heat sources due to enthalpy changes should be taken into account, therefore the unsteady heat equation is:

$$\frac{\partial^2 T_{tot}^{(i)}}{\partial r^2} + \frac{1}{r} \frac{\partial T_{tot}^{(i)}}{\partial r} - \frac{1}{D^{(i)}} \frac{\partial T_{tot}^{(i)}}{\partial t} = - \sum_{p=1}^{N_p} \frac{\Delta H_p(T)}{\lambda^{(i)}} \dot{X}_p^{(i)} \quad (1)$$

where as a general rule in the following, the superscript (i) is related to the i -th layer, $n+1$ is the total number of layers, $T_{tot}^{(i)}$ is the total temperature in the i -th layer, $D^{(i)}$ the thermal diffusivity, $\lambda^{(i)}$ the thermal conductivity, N_p the number of produced phases, ΔH_p the temperature dependent enthalpy change associated to the p -th phase change and $\dot{X}_p^{(i)}$ the p -th phase proportion rate. This partial differential equation is nonlinear because of the temperature dependent right-side term. However thermal conductivity and diffusivity are assumed to be temperature independent, so that the homogenous partial differential equation is linear. The strategy to deal with non-linearity relies on the coupling scheme that consists in alternating heat conduction problem with known heat sources and multiphase change problem with known temperature field. Iterations (starting from an initial guess) are carried out to capture the temperature dependence of heat sources. The temperature dependent right-side term is then replaced by known time and space dependent heat sources and the inhomogeneous equation becomes linear. Therefore, the total solution can be decomposed into an homogenous solution $T^{(i)}$ of the heat equation without right-side term (3) and a particular solution $\widehat{T}^{(i)}$:

$$T_{tot}^{(i)} = T^{(i)} + \widehat{T}^{(i)} \quad (2)$$

2.1. Homogenous heat equation

The homogenous heat equation is written as follows:

$$\frac{\partial^2 T^{(i)}}{\partial r^2} + \frac{1}{r} \frac{\partial T^{(i)}}{\partial r} - \frac{1}{D^{(i)}} \frac{\partial T^{(i)}}{\partial t} = 0 \quad (3)$$

By using separation of variables techniques considering time and space dependencies, time dependency only and space dependency only, an analytical solution can be written as follows:

$$T^{(i)}(r, t) = \sum_{k=1}^{N_k} \left[\Theta_k^{(i)} J_0 \left(\frac{\beta_k}{\sqrt{D^{(i)}}} r \right) + \underline{\Theta}_k^{(i)} Y_0 \left(\frac{\beta_k}{\sqrt{D^{(i)}}} r \right) \right] \exp(-\beta_k^2 t) + \Gamma^{(i)} \ln \left(\frac{r}{r^{(i)}} \right) + \underline{\Gamma}^{(i)} \quad (4)$$

where J_0 and Y_0 are the 0-order Bessel functions of the first and second kind respectively, β_k are unknown eigenvalues and $\Theta_k^{(i)}$, $\underline{\Theta}_k^{(i)}$, $\Gamma^{(i)}$, $\underline{\Gamma}^{(i)}$ are unknown coefficients. Boundary conditions are temperature and heat flux continuities through all interfaces and heat flux conditions using heat transfer coefficients at both inner and outer surfaces. Thus (for $i \in \{0, \dots, n-1\}$):

$$\left\{ \begin{array}{ll} [0] & : \lambda^{(0)} \frac{\partial T^{(0)}}{\partial r}(r^{(0)}, t) = H^{(0)} (T^{(0)}(r^{(0)}, t) - T_{int}) \\ [i]_T & : T^{(i)}(r^{(i+1)}, t) = T^{(i+1)}(r^{(i+1)}, t) \\ [i]_H & : \lambda^{(i)} \frac{\partial T^{(i)}}{\partial r}(r^{(i+1)}, t) = \lambda^{(i+1)} \frac{\partial T^{(i+1)}}{\partial r}(r^{(i+1)}, t) \\ [n] & : \lambda^{(n)} \frac{\partial T^{(n)}}{\partial r}(r^{(n+1)}, t) = -H^{(n+1)} (T^{(n)}(r^{(n+1)}, t) - T_{ext}) \end{array} \right. \quad (5)$$

Of course boundary conditions of the particular solution $\widehat{T}^{(i)}$ should be consistent with (5) so that the total problem verifies also (5) that is to say that $\widehat{T}^{(i)}$ should also verify $[i]_T$ and $[i]_H$ but the surrounding temperature should vanish in conditions $[0]$ and $[n]$ of (5) as detailed in (19). By plugging (4) into (5) it is obtained on the one hand:

$$\left\{ \begin{array}{l} \Theta_k^{(0)} \left[\lambda^{(0)} \frac{\beta_k}{\sqrt{D^{(0)}}} J'_0 \left(\frac{\beta_k}{\sqrt{D^{(0)}}} r^{(0)} \right) - H^{(0)} J_0 \left(\frac{\beta_k}{\sqrt{D^{(0)}}} r^{(0)} \right) \right] + \\ \underline{\Theta}_k^{(0)} \left[\lambda^{(0)} \frac{\beta_k}{\sqrt{D^{(0)}}} Y'_0 \left(\frac{\beta_k}{\sqrt{D^{(0)}}} r^{(0)} \right) - H^{(0)} Y_0 \left(\frac{\beta_k}{\sqrt{D^{(0)}}} r^{(0)} \right) \right] = 0 \\ \\ \Theta_k^{(i)} J_0 \left(\frac{\beta_k}{\sqrt{D^{(i)}}} r^{(i+1)} \right) + \underline{\Theta}_k^{(i)} Y_0 \left(\frac{\beta_k}{\sqrt{D^{(i)}}} r^{(i+1)} \right) \\ - \Theta_k^{(i+1)} J_0 \left(\frac{\beta_k}{\sqrt{D^{(i+1)}}} r^{(i+1)} \right) - \underline{\Theta}_k^{(i+1)} Y_0 \left(\frac{\beta_k}{\sqrt{D^{(i+1)}}} r^{(i+1)} \right) = 0 \\ \\ \Theta_k^{(i)} \lambda^{(i)} \frac{\beta_k}{\sqrt{D^{(i)}}} J'_0 \left(\frac{\beta_k}{\sqrt{D^{(i)}}} r^{(i+1)} \right) + \underline{\Theta}_k^{(i)} \lambda^{(i)} \frac{\beta_k}{\sqrt{D^{(i)}}} Y'_0 \left(\frac{\beta_k}{\sqrt{D^{(i)}}} r^{(i+1)} \right) \\ - \Theta_k^{(i+1)} \lambda^{(i+1)} \frac{\beta_k}{\sqrt{D^{(i+1)}}} J'_0 \left(\frac{\beta_k}{\sqrt{D^{(i+1)}}} r^{(i+1)} \right) - \underline{\Theta}_k^{(i+1)} \lambda^{(i+1)} \frac{\beta_k}{\sqrt{D^{(i+1)}}} Y'_0 \left(\frac{\beta_k}{\sqrt{D^{(i+1)}}} r^{(i+1)} \right) = 0 \\ \\ \Theta_k^{(n)} \left[\lambda^{(n)} \frac{\beta_k}{\sqrt{D^{(n)}}} J'_0 \left(\frac{\beta_k}{\sqrt{D^{(n)}}} r^{(n+1)} \right) + H^{(n+1)} J_0 \left(\frac{\beta_k}{\sqrt{D^{(n)}}} r^{(n+1)} \right) \right] + \\ \underline{\Theta}_k^{(n)} \left[\lambda^{(n)} \frac{\beta_k}{\sqrt{D^{(n)}}} Y'_0 \left(\frac{\beta_k}{\sqrt{D^{(n)}}} r^{(n+1)} \right) + H^{(n+1)} Y_0 \left(\frac{\beta_k}{\sqrt{D^{(n)}}} r^{(n+1)} \right) \right] = 0 \end{array} \right. \quad (6)$$

and on the other hand:

$$\left\{ \begin{array}{l} \Gamma^{(0)} \frac{\lambda^{(0)}}{r^{(0)}} - \underline{\Gamma}^{(0)} H^{(0)} = -H^{(0)} T_{int} \\ \Gamma^{(i)} \ln \left(\frac{r^{(i+1)}}{r^{(i)}} \right) + \underline{\Gamma}^{(i)} - \underline{\Gamma}^{(i+1)} = 0 \\ \Gamma^{(i)} \lambda^{(i)} - \Gamma^{(i+1)} \lambda^{(i+1)} = 0 \\ \Gamma^{(n)} \left(\frac{\lambda^{(n)}}{r^{(n+1)}} + H^{(n+1)} \ln \left(\frac{r^{(n+1)}}{r^{(n)}} \right) \right) + H^{(n+1)} \underline{\Gamma}^{(n)} = H^{(n+1)} T_{ext} \end{array} \right. \quad (7)$$

From both systems (6) and (7) one obtains:

$$\underline{H}_k \cdot \underline{\Theta}_k = \mathbf{0} \quad (8)$$

$$\underline{h} \cdot \underline{\Gamma} = F \quad (9)$$

where:

$$\left\{ \begin{array}{l} \underline{\Theta}_k = (\Theta_k^{(0)}, \underline{\Theta}_k^{(0)}, \dots, \Theta_k^{(n)}, \underline{\Theta}_k^{(n)})^T \\ \underline{\Gamma} = (\Gamma^{(0)}, \underline{\Gamma}^{(0)}, \dots, \Gamma^{(n)}, \underline{\Gamma}^{(n)})^T \\ F = (-H^{(0)} T_{int}, 0, \dots, 0, H^{(n+1)} T_{ext})^T \end{array} \right. \quad (10)$$

where \underline{H}_k (that depends explicitly on β_k) and \underline{h} are matrices of size $2(n+1) \times 2(n+1)$ clearly defined by (6) and (7). These matrices are of the form:

$$\begin{pmatrix} H_{1,1} & H_{1,2} & 0 & 0 & 0 & 0 & \cdots & 0 & 0 & 0 & 0 \\ H_{2,1} & H_{2,2} & -H_{2,3} & -H_{2,4} & 0 & 0 & \cdots & 0 & 0 & 0 & 0 \\ H_{3,1} & H_{3,2} & -H_{3,3} & -H_{3,4} & 0 & 0 & \cdots & 0 & 0 & 0 & 0 \\ 0 & 0 & H_{4,3} & H_{4,4} & -H_{4,5} & -H_{4,6} & \cdots & 0 & 0 & 0 & 0 \\ 0 & 0 & H_{5,3} & H_{5,4} & -H_{5,5} & -H_{5,6} & \cdots & 0 & 0 & 0 & 0 \\ & & & & & & \vdots & & & & \\ 0 & 0 & 0 & 0 & 0 & 0 & \cdots & H_{2n,2n-1} & H_{2n,2n} & -H_{2n,2n+1} & -H_{2n,2n+2} \\ 0 & 0 & 0 & 0 & 0 & 0 & \cdots & H_{2n+1,2n-1} & H_{2n+1,2n} & -H_{2n+1,2n+1} & -H_{2n+1,2n+2} \\ 0 & 0 & 0 & 0 & 0 & 0 & \cdots & 0 & 0 & H_{2n+2,2n+1} & H_{2n+2,2n+2} \end{pmatrix} \quad (11)$$

The system (9) can be solved easily, since \underline{h} does not depend on eigenvalues and is invertible. Conditioning issues may arise because of very severe contrasts with respect to layer thicknesses and material properties. Indeed, applications to steel layers with very thin air gaps are considered. This can be regularized by increasing slightly the thermal conductivity of air gaps (it should remain insulating compared with steel). Therefore, the equivalent air gap thickness derived in section 5 increases, reducing both geometrical and material contrasts. Thus, coefficients $\Gamma^{(i)}$ and $\underline{\Gamma}^{(i)}$ reads:

$$\underline{\Gamma} = \underline{h}^{-1} \cdot \underline{F} \quad (12)$$

However, a non-trivial solution of (8) can be found if and only if the matrix determinant vanishes. Therefore eigenvalues β_k are determined by finding positive successive roots of the determinant of the matrix \underline{H}_k . The higher N_k is chosen and better the initial condition is verified. The rank of the matrix \underline{H}_k is $2n+1$, therefore the solution set is a one-dimensional vector space that can be parametrized by $\Theta_k^{(0)}$ considered as a right-side term. The last equation of (6) being automatically verified, the system (8) reduces to (for $i \in \{0, \dots, n\}$):

$$\begin{cases} \Theta_k^{(i)} = \Theta_k^{(0)} \alpha_k^{(i)} \\ \underline{\Theta}_k^{(i)} = \Theta_k^{(0)} \underline{\alpha}_k^{(i)} \end{cases} \quad (13)$$

where:

$$\begin{cases} \alpha_k^{(0)} = 1 \\ \underline{\alpha}_k^{(0)} = -\frac{H_{1,1}}{H_{1,2}} \end{cases} \quad (14)$$

and where the following recursive formula holds (for $i \in \{0, \dots, n-1\}$):

$$\begin{pmatrix} \alpha_k^{(i+1)} \\ \underline{\alpha}_k^{(i+1)} \end{pmatrix} = \begin{pmatrix} H_{2i+2,2i+3} & H_{2i+2,2i+4} \\ H_{2i+3,2i+3} & H_{2i+3,2i+4} \end{pmatrix}^{-1} \cdot \begin{pmatrix} H_{2i+2,2i+1} & H_{2i+2,2i+2} \\ H_{2i+3,2i+1} & H_{2i+3,2i+2} \end{pmatrix} \cdot \begin{pmatrix} \alpha_k^{(i)} \\ \underline{\alpha}_k^{(i)} \end{pmatrix} \quad (15)$$

Therefore the temperature field reduces to:

$$T^{(i)}(r, t) = \sum_{k=1}^{N_k} \Theta_k^{(0)} \left[\alpha_k^{(i)} J_0 \left(\frac{\beta_k}{\sqrt{D^{(i)}}} r \right) + \underline{\alpha}_k^{(i)} Y_0 \left(\frac{\beta_k}{\sqrt{D^{(i)}}} r \right) \right] \exp(-\beta_k^2 t) + \Gamma^{(i)} \ln \left(\frac{r}{r^{(i)}} \right) + \underline{\Gamma}^{(i)} \quad (16)$$

The only remaining unknowns are coefficients $\Theta_k^{(0)}$. The determination of these latter coefficients is done by using the following initial condition $T_{tot}^{(i)}(r, t=0) = T_{ini}(r)$ where $T_{ini}(r)$ is the initial temperature field. This determination is done in section 2.3.

2.2. Particular solution

The particular solution $\widehat{T}^{(i)}$ verifies the heat equation (1) accounting for the right-side term. Phase proportion rates $\dot{X}_p^{(i)}(r, t)$ are obtained numerically in section 3. An analytic form is needed for the heat equation. Therefore, an expansion into decreasing exponential series is used:

$$-\frac{\Delta H_p(T)}{\lambda^{(i)}} \dot{X}_p^{(i)}(r, t) = \sum_{k=1}^{\widehat{N}_k} \chi_{p,k}^{(i)}(r) \exp(-\widehat{\beta}_k^2 t) + \chi_{p,0}^{(i)}(r) \quad (17)$$

Eigenvalues are arbitrarily chosen such as the data fit procedure is accurate and such as $\widehat{\beta}_k \neq \beta_k$ so that the associated matrix is well conditioned. This new set of eigenvalues are not roots of any equation and does not cost additional computation time. In this paper $\widehat{\beta}_k$ are chosen in the middle of successive β_k . Coefficients $\chi_{p,k}^{(i)}(r)$ are computed numerically using data fit procedures. It is possible to deal with the r -dependance by using specific orthogonal basis functions presented in Appendix A. However technicalities can be avoided by considering that phase changes are homogenous in each steel layer which is rather well verified considering that steel layers are quite thin (1 or 2 mm). This assumption also enables to avoid a discretization along the radial direction for the multiphase change model presented in section 3. Therefore, in the following, the r -dependance is discarded but a more general solution is addressed in Appendix A. Moreover it should be noted that the analytical form (17) is only an approximation of the heat source because of the data fit procedure. By using separation of variables techniques considering time and space dependencies, time dependency only and space dependency only, a particular solution can be written as follows:

$$\begin{aligned} \widehat{T}^{(i)}(r, t) = & \sum_{k=1}^{\widehat{N}_k} \left[\widehat{\Theta}_k^{(i)} J_0 \left(\frac{\widehat{\beta}_k}{\sqrt{D^{(i)}}} r \right) + \widehat{\Theta}_k^{(i)} Y_0 \left(\frac{\widehat{\beta}_k}{\sqrt{D^{(i)}}} r \right) + \sum_{p=1}^{N_p} \chi_{p,k}^{(i)} \frac{D^{(i)}}{\widehat{\beta}_k^2} \right] \exp(-\widehat{\beta}_k^2 t) \\ & + \widehat{\Gamma}^{(i)} \ln \left(\frac{r}{r^{(i)}} \right) + \widehat{\Gamma}^{(i)} + \frac{\chi_{p,0}^{(i)}}{4} r^2 \end{aligned} \quad (18)$$

where $\widehat{\Theta}_k^{(i)}$ and $\widehat{\Gamma}^{(i)}$ are unknown. It should be noted that most parts of the latter form (18) are solutions of the homogenous heat conduction problem, only terms involving $\chi_{p,k}^{(i)}$ are truly inhomogeneous solutions. The particular solution should verify the following boundary conditions (for $i \in \{0, \dots, n-1\}$):

$$\left\{ \begin{array}{ll} [0] & : \lambda^{(0)} \frac{\partial \widehat{T}^{(0)}}{\partial r}(r^{(0)}, t) = H^{(0)} \widehat{T}^{(0)}(r^{(0)}, t) \\ [i]_T & : \widehat{T}^{(i)}(r^{(i+1)}, t) = \widehat{T}^{(i+1)}(r^{(i+1)}, t) \\ [i]_H & : \lambda^{(i)} \frac{\partial \widehat{T}^{(i)}}{\partial r}(r^{(i+1)}, t) = \lambda^{(i+1)} \frac{\partial \widehat{T}^{(i+1)}}{\partial r}(r^{(i+1)}, t) \\ [n] & : \lambda^{(n)} \frac{\partial \widehat{T}^{(n)}}{\partial r}(r^{(n+1)}, t) = -H^{(n+1)} \widehat{T}^{(n)}(r^{(n+1)}, t) \end{array} \right. \quad (19)$$

Boundary conditions (19) can be written as follows:

$$\underline{\widehat{H}}_k \cdot \widehat{\Theta}_k = \widehat{F}_k \quad \text{and} \quad \underline{h} \cdot \widehat{\Gamma} = \widehat{F} \quad (20)$$

where:

$$\begin{cases} \widehat{\Theta}_k = \left(\widehat{\Theta}_k^{(0)}, \widehat{\Theta}_k^{(0)}, \dots, \widehat{\Theta}_k^{(n)}, \widehat{\Theta}_k^{(n)} \right)^T \\ \widehat{\Gamma} = \left(\widehat{\Gamma}^{(0)}, \widehat{\Gamma}^{(0)}, \dots, \widehat{\Gamma}^{(n)}, \widehat{\Gamma}^{(n)} \right)^T \end{cases} \quad (21)$$

and where:

$$\widehat{\mathbf{F}}_k = \begin{pmatrix} H^{(0)} \sum_{p=1}^{N_p} \chi_{p,k}^{(0)} \frac{D^{(0)}}{\widehat{\beta}_k^2} \\ \vdots \\ \sum_{p=1}^{N_p} \chi_{p,k}^{(i+1)} \frac{D^{(i+1)}}{\widehat{\beta}_k^2} - \chi_{p,k}^{(i)} \frac{D^{(i)}}{\widehat{\beta}_k^2} \\ 0 \\ \vdots \\ -H^{(n+1)} \sum_{p=1}^{N_p} \chi_{p,k}^{(n)} \frac{D^{(n)}}{\widehat{\beta}_k^2} \end{pmatrix} \quad \text{and} \quad \widehat{\mathbf{F}} = \begin{pmatrix} \sum_{p=1}^{N_p} \frac{\chi_{p,0}^{(0)}}{2} r^{(0)} \left(H^{(0)} \frac{r^{(0)}}{2} - \lambda^{(0)} \right) \\ \vdots \\ \sum_{p=1}^{N_p} \frac{\chi_{p,0}^{(i+1)} - \chi_{p,0}^{(i)}}{4} (r^{(i+1)})^2 \\ \sum_{p=1}^{N_p} \frac{\lambda^{(i+1)} \chi_{p,0}^{(i+1)} - \lambda^{(i)} \chi_{p,0}^{(i)}}{2} r^{(i+1)} \\ \vdots \\ - \sum_{p=1}^{N_p} \frac{\chi_{p,0}^{(n)}}{2} \left(H^{(n+1)} \frac{r^{(n+1)}}{2} + \lambda^{(n)} \right) \end{pmatrix} \quad (22)$$

Eventually $\widehat{\Theta}_k$ and $\widehat{\Gamma}$ are determined easily by inverting matrices $\widehat{\mathbf{H}}_k$ and \mathbf{h} . Thus:

$$\widehat{\Theta}_k = \widehat{\mathbf{H}}_k^{-1} \cdot \widehat{\mathbf{F}}_k \quad \text{and} \quad \widehat{\Gamma} = \mathbf{h}^{-1} \cdot \widehat{\mathbf{F}} \quad (23)$$

2.3. Initial condition

The initial condition $T_{tot}^{(i)}(r, t = 0) = T_{ini}(r)$ is finally used in order to determine the only remaining unknown coefficients $\Theta_k^{(0)}$. This process relies on a particular orthogonality relation related to the following scalar product:

$$\langle f_1, f_2 \rangle = \sum_{i=0}^n \frac{\lambda^{(i)}}{D^{(i)}} \int_{r^{(i)}}^{r^{(i+1)}} r f_1(r) f_2(r) dr \quad (24)$$

Consider the following basis functions defined on the whole multilayer composite:

$$f_k(r) = \alpha_k^{(i)} J_0 \left(\frac{\beta_k}{\sqrt{D^{(i)}}} r \right) + \alpha_k^{(i)} Y_0 \left(\frac{\beta_k}{\sqrt{D^{(i)}}} r \right) \quad \text{with } r \in [r^{(i)}, r^{(i+1)}] \quad (25)$$

Therefore, the following orthogonality relation holds as demonstrated by De Monte [2]:

$$\langle f_k, f_l \rangle = \begin{cases} 0 & \text{if } k \neq l \\ M_k > 0 & \text{if } k = l \end{cases} \quad (26)$$

The basis functions $(f_k)_{k \in \{1, \dots, N_k\}}$ form an orthogonal basis with respect to the latter scalar product. Therefore coefficients $(\Theta_k^{(0)})_{k \in \{1, \dots, N_k\}}$ are determined by an orthogonal projection of the initial condition on the orthogonal basis. More precisely, the initial condition reads:

$$\sum_{k=1}^{N_k} \Theta_k^{(0)} \left[\alpha_k^{(i)} J_0 \left(\frac{\beta_k}{\sqrt{D^{(i)}}} r \right) + \alpha_k^{(i)} Y_0 \left(\frac{\beta_k}{\sqrt{D^{(i)}}} r \right) \right] + \Gamma^{(i)} \ln \left(\frac{r}{r^{(i)}} \right) + \Gamma^{(i)} + \widehat{T}^{(i)}(r, t = 0) = T_{ini}^{(i)}(r) \quad (27)$$

Hence:

$$\sum_{k=1}^{N_k} \Theta_k^{(0)} f_k(r) = f_{ini}(r) \quad (28)$$

where f_{ini} is defined on the whole multilayer composite as follows:

$$f_{ini}(r) = T_{ini}^{(i)}(r) - \Gamma^{(i)} \ln\left(\frac{r}{r^{(i)}}\right) - \underline{\Gamma}^{(i)} - \widehat{T}^{(i)}(r, t = 0) \text{ with } r \in [r^{(i)}, r^{(i+1)}] \quad (29)$$

Therefore, following coefficients are found:

$$\Theta_k^{(0)} = \frac{\langle f_{ini}, f_k \rangle}{\langle f_k, f_k \rangle} \quad (30)$$

3. Multiphase change problem

As described in section 1.3, each phase transformation occur within a temperature range. Austenite is stable above Ae_3 . Ferrite is formed between Ae_3 and Ae_1 and the equilibrium phase proportion between austenite and ferrite can be evaluated by using the lever rule on the thermodynamic equilibrium phase diagram. Pearlite is formed between Ae_1 and BS, bainite is then formed between BS and MS, and martensite is formed below MS. Ferrite, pearlite, bainite and martensite are formed from retained austenite. Thus, when all austenite has been consumed, phase transformation stops. The classical equation that describes the overall phase transformation kinetics under isothermal assumption proposed by Avrami [18] is written as follows (for $p = 1, 2, 3$ i.e., ferrite, pearlite and bainite):

$$X_p^{iso}(t) = 1 - \exp(-k_p(T)t^{n_p}) \quad (31)$$

where the superscript *iso* means *isotherm*. Consider a non-isotherm path given by $t' \mapsto T(t')$. Let t be a fixed time and t' be any time in the interval $[0, t]$. The phase proportion produced with the non-isothermal condition during the time interval $[0, t]$ is denoted by $X_p(t)$. Let t_{iso} denotes the time that would be necessary to produce the same phase proportion under isothermal assumption with the following constant temperature $T^* = T(t')$ (it depends explicitly on $T(t')$ but for sake of conciseness the notation is kept simple). Thus $X_p^{iso}(t_{iso}) = X_p(t)$. Using (31) one can write:

$$t_{iso} = \left(-\frac{\ln(1 - X_p(t))}{k_p(T(t'))} \right)^{\frac{1}{n_p}} \quad (32)$$

The isokinetic assumption enables to write:

$$\int_0^t \frac{dt'}{t_{iso}} = 1 \quad (33)$$

By using (32) and (33) one obtains:

$$X_p(t) = 1 - \exp\left(-\left[\int_0^t k_p(T(t'))^{\frac{1}{n_p}} dt'\right]^{n_p}\right) \quad (34)$$

The phase proportion rate is calculated as follows:

$$\dot{X}_p(t) = n_p k_p(T(t))^{\frac{1}{n_p}} \left[\int_0^t k_p(T(t'))^{\frac{1}{n_p}} dt' \right]^{n_p-1} \exp\left(-\left[\int_0^t k_p(T(t'))^{\frac{1}{n_p}} dt'\right]^{n_p}\right) \quad (35)$$

For martensite transformation (i.e., $p = 4$) the phase proportion is calculated as proposed by Koistinen and Marburger [21]:

$$X_4(t) = X_{ra}(t) [1 - \exp(-\alpha (T - MS))] \quad (36)$$

where X_{ra} is the retained austenite and α a constant parameter set to 0.01 in this paper.

4. Coupling

In this paper, the coupling scheme consists simply on alternating both the heat conduction problem with known phase proportion rates and the multiphase change problem with known temperature field. The alternating coupling algorithm is simply depicted in figure 4. Convergence is tested on the temperature field and the tolerance is set to 5 K. The algorithm begins with zero phase proportion rates (i.e., no heat source). A first temperature estimation is produced and the multiphase change problem is carried out on this basis, giving the first estimation of heat sources. This scheme is repeated until convergence. No mathematical proof of convergence is broached in this paper. But practically, for the present coupled problem, this procedure converges within a very few iterations as shown for instance in figure 5 that is computed from the practical example presented in section 7.

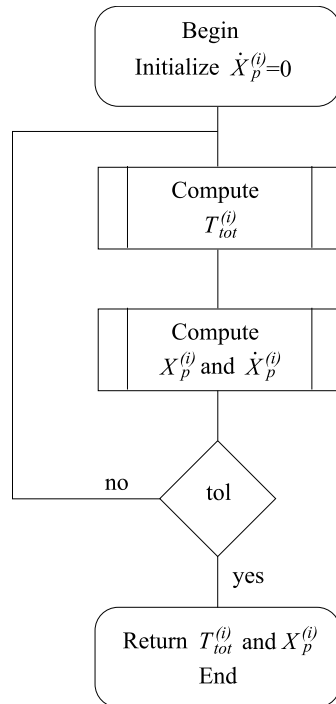


Figure 4: Coupling algorithm

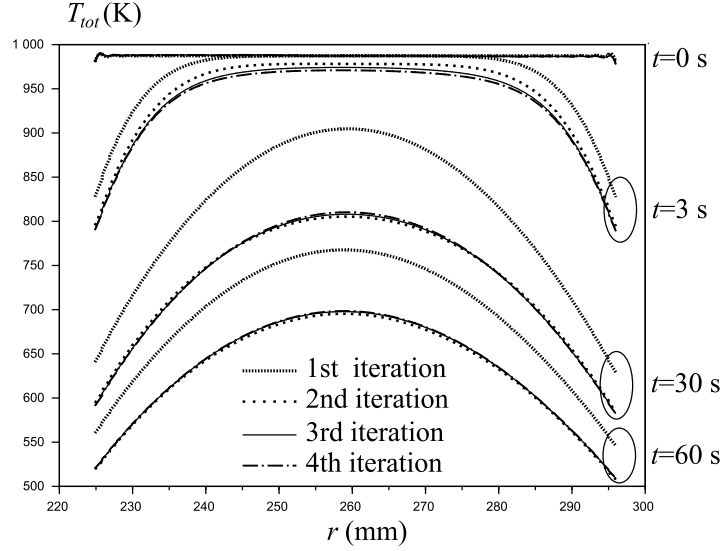


Figure 5: Convergence at $Z = 0$

5. Equivalent air gap thickness

As detailed in section 1.2, thermal contact resistance is modeled by introducing air gaps between steel layers. Therefore, the solution derived in section 2, that relies on temperature and heat flux continuities through each interface, can be used by alternating steel and thin air layers. The equivalent air gap thickness is determined by ensuring that the average heat flux through the air gap matches the heat flux at the imperfect steel/steel interface modeled by thermal contact resistance. Thermal contact resistance is defined by H that depends on contact pressure and roughness parameters. The heat flux at the imperfect interface is classically:

$$Q = H (T_2(t) - T_1(t)) \quad (37)$$

where $T_1(t)$ and $T_2(t)$ are the temperatures at lower and upper surfaces of the interface as depicted in figure 6. The equivalent air gap thickness denoted by th is defined as shown in figure 6, that is to say that temperatures at lower and upper surfaces of the air gap are also $T_1(t)$ and $T_2(t)$. In addition, temperature and heat flux continuities are ensured. Consider that $T_1(t)$ and $T_2(t)$ can be written as follows (for $j = 1$ or 2):

$$T_j(t) = \int_0^{+\infty} \mathcal{T}_j(\beta) \exp(-\beta^2 t) d\beta + T_j^0 \quad (38)$$

Consider T_a , D_a and λ_a the temperature, thermal diffusivity and thermal conductivity in the air gap¹. A simple equivalent thickness is found by solving the heat conduction problem in Cartesian coordinates:

$$\frac{\partial^2 T_a}{\partial x^2} = \frac{1}{D_a} \frac{\partial T_a}{\partial t} \quad (39)$$

¹Insulating properties should be considered but not necessarily those of air.

Separation of variables techniques enable to write a general solution as follows:

$$T_a(x, t) = \int_0^{+\infty} \left(A(\beta) \cos\left(\frac{\beta}{\sqrt{D_a}}x\right) + B(\beta) \sin\left(\frac{\beta}{\sqrt{D_a}}x\right) \right) \exp(-\beta^2 t) d\beta + A^0 x + B^0 \quad (40)$$

Boundary conditions are:

$$\begin{cases} T_a\left(-\frac{th}{2}, t\right) = T_1(t) \\ T_a\left(\frac{th}{2}, t\right) = T_2(t) \end{cases} \quad (41)$$

Hence:

$$\begin{cases} A(\beta) = \frac{T_2(\beta) + T_1(\beta)}{2 \cos\left(\frac{\beta}{\sqrt{D_a}} \frac{th}{2}\right)} & A^0 = \frac{T_2^0 - T_1^0}{th} \\ B(\beta) = \frac{T_2(\beta) - T_1(\beta)}{2 \sin\left(\frac{\beta}{\sqrt{D_a}} \frac{th}{2}\right)} & B^0 = \frac{T_2^0 + T_1^0}{2} \end{cases} \quad (42)$$

The equivalent air gap thickness is determined by ensuring that the average heat flux through the air gap matches the heat flux at the imperfect interface defined by (37), therefore:

$$\begin{cases} H(T_2(\beta) - T_1(\beta)) = \frac{\lambda_a}{th} \frac{\beta}{\sqrt{D_a}} \int_{-\frac{th}{2}}^{\frac{th}{2}} \left(-A(\beta) \sin\left(\frac{\beta}{\sqrt{D_a}}x\right) + B(\beta) \cos\left(\frac{\beta}{\sqrt{D_a}}x\right) \right) dx \\ \quad = \frac{2\lambda_a B(\beta) \sin\left(\frac{\beta}{\sqrt{D_a}} \frac{th}{2}\right)}{th} \\ \quad = \frac{\lambda_a (T_2(\beta) - T_1(\beta))}{th} \\ H(T_2^0 - T_1^0) = \frac{\lambda_a}{th} \int_{-\frac{th}{2}}^{\frac{th}{2}} A^0 dx = \lambda_a A^0 = \frac{\lambda_a (T_2^0 - T_1^0)}{th} \end{cases} \quad (43)$$

Thus, the equivalent air gap thickness is:

$$th = \frac{\lambda_a}{H} \quad (44)$$

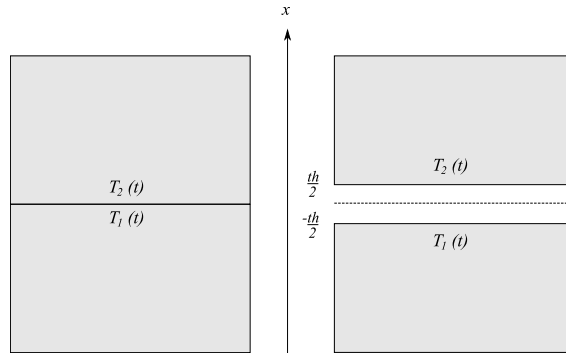


Figure 6: Air gap thickness

In this paper, thermal contact resistance is extracted from the work of Kaza [9] but other formulations are also possible:

$$H = \frac{\lambda_s}{R_q} \left(2.16 \left(\frac{P}{3.3\sigma_Y + P} \right)^{0.51} + 0.36 \frac{\lambda_a}{\lambda_s} \right) \quad (45)$$

where λ_s and λ_a are thermal conductivities of steel and air respectively, P is the local contact pressure, σ_Y the yield stress and R_q the quadratic roughness parameter (average high of asperities).

6. Validation

In this section, exactness of the analytical solution developed in section 2 (considering the particular solution related to heat sources) is demonstrated by comparing results with a Finite Element model. Thus, an axisymmetric composite, alternating 2 mm thick steel layers with 5 μ m thick air layers, is modeled using the freeware Cast3m (<http://www-cast3m.cea.fr/>). Details are listed in table 1. Heat sources are directly imposed in steel layers as a known function $P(r, t)$ in W.mm^{-3} corresponding to $\Delta H_p \dot{X}_p^{(i)}$ in (1):

$$P(r, t) = 0.5 \times t(t - 2.5) \times (r - 200)(r - 220)/100 \quad (46)$$

Thus, the coupling problem consisting in computing the heat source as a function of the previous temperature field estimation is not reproduced by FEM. Here, only the analytical solution that gives the temperature field for a known heat source is validated. Validation of the coupling procedure has been done simply by showing convergence within a very few iterations. Comparison is presented in figure 7 and perfect agreement is observed (it should be mentioned that only half of the Finite Element points are drawn for clarity reasons).

Table 1: Comparison parameters

	Steel	Air gap
Number of layers	10	9
Thickness (mm)	2	0.005
Thermal conductivity ($\text{J.s}^{-1}.\text{mm}^{-1}.\text{K}^{-1}$)	50×10^{-3}	0.026×10^{-3}
Density (g.mm^{-3})	7850×10^{-6}	1.293×10^{-6}
Heat capacity ($\text{J.g}^{-1}.\text{K}^{-1}$)	0.5308	1.0054
Thermal diffusivity ($\text{mm}^2.\text{s}^{-1}$)	12	20

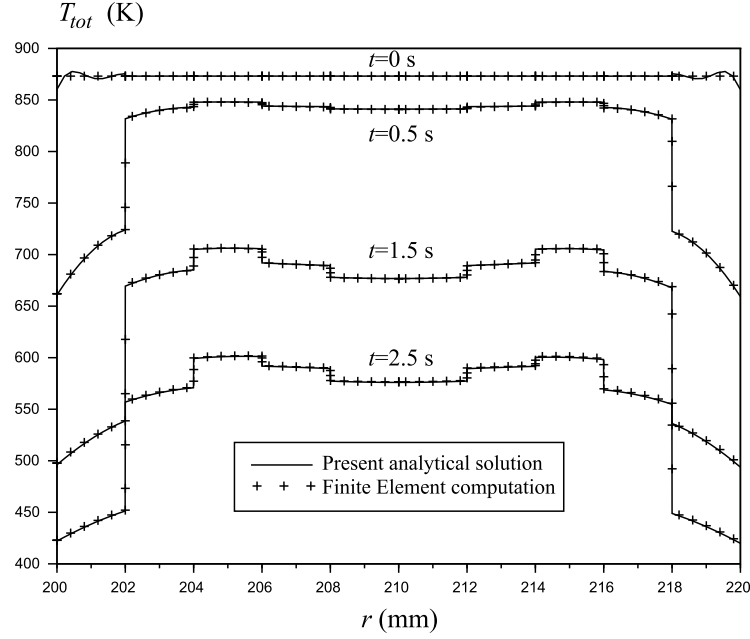


Figure 7: Comparison with FEM

7. First numerical results

Phase change temperatures Ae_3 , Ae_1 , BS and MS have been extracted from Lee et al. [29]. Parameters k_p and n_p in the multiphase change problem described in section multiphase have been extracted from Hawbolt et al. [30] for austenite to ferrite and austenite to pearlite transformations for a 1025 steel whose composition is listed in table 2. For austenite to bainite transformation, parameters have been extracted from Han et al. [31]. Continuous cooling tests presented in figure 8 have been carried out at two different cooling rates, namely 5 K/s and 20 K/s. Enthalpy changes during phase transformation are in general temperature dependent. But for the following example constant values are chosen and give an order of magnitude and do not represent a specific steel. For austenite to ferrite, pearlite and bainite transformations $\Delta H_p = -0.4 \text{ J.mm}^{-3}$ ($p = 1, 2, 3$) and for austenite to martensite transformation $\Delta H_4 = -0.3 \text{ J.mm}^{-3}$.

In the previous paper of Weisz-Patrault et al. [24], the coiling process has been modeled and 70 wraps have been computed considering a yield stress $\sigma_Y = 600 \text{ MPa}$ and a roughness parameter $R_q = 5 \text{ }\mu\text{m}$. Contact pressures and final geometry are extracted and used as inputs for the present study. A simple elastic calculation is done to simulate that the mandrel is removed, applying on the coil internal surface the opposite contact pressure between the mandrel and the first layer. Resulting contact pressures along the radial direction of the coil are presented in figure 9 for several axial positions. The final geometry is obtained by introducing air gaps between all steel layers according to (44) and (45). When contact pressure vanishes, surfaces are not in contact and then the real air gap is considered. Moreover, the initial temperature is set to 987 K and the surrounding temperature is 293.15 K. Heat transfer coefficients are $H^{(0)} = H^{(n+1)} = 0.002 \text{ W.mm}^{-2}.\text{K}^{-1}$. The model is applied for each axial position.

Table 2: Composition of 1025 Steel (weight %)

C	Mn	Si	S	P
0.25	0.46	0.21	0.014	0.018

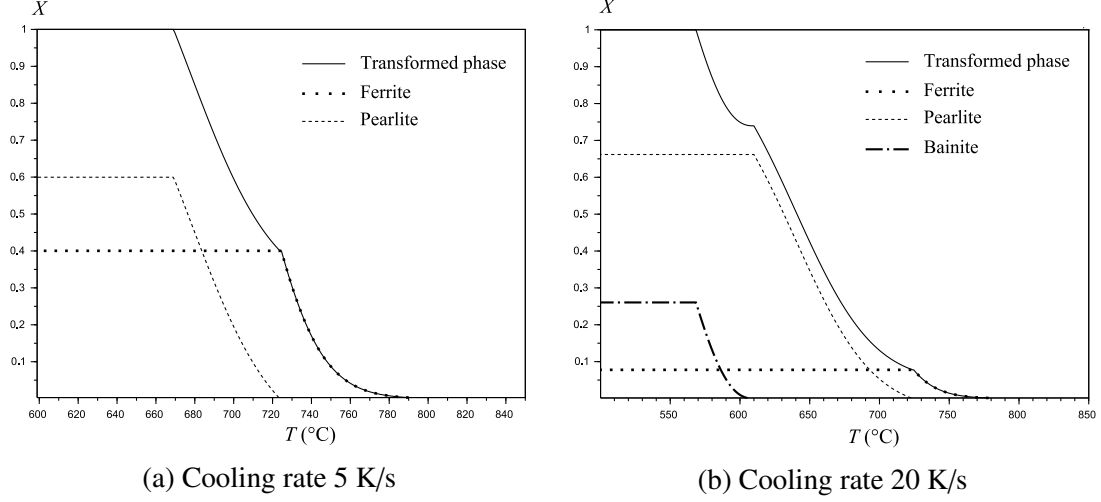


Figure 8: Continuous cooling test

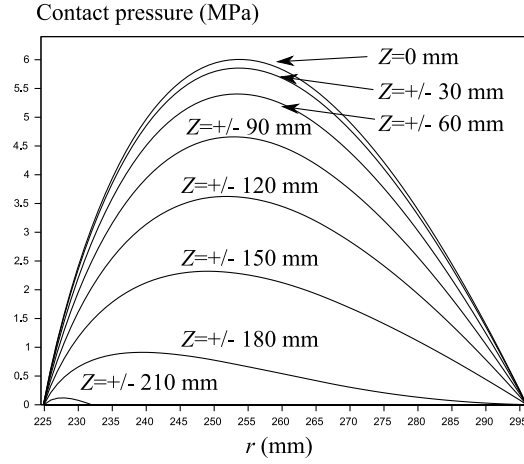


Figure 9: Contact pressure at different axial positions

Temperature maps are presented in figure 10. Since the coil is cooled by internal and external surfaces, the center cools down much slower than near boundaries. The initial temperature being slightly lower than A_{e1} (pearlite start temperature), pearlite then bainite are produced without producing ferrite. All austenite has been consumed therefore no martensite can be formed when the temperature reaches the martensite temperature start M_s . Phase proportion maps are presented in figures 11a and 11b. The time scale has been chosen so that evolutions are visible. It should be noticed that the amount of formed pearlite is more significant at the center than near the internal and external surfaces because the temperature range where pearlite can be formed is maintained longer. However for $t = 6$ s and $t = 9$ s, one can observe that the

maximum phase proportion of pearlite is not at the center. This is due to phase transformation kinetics. Indeed, phase transformation is slower when the temperature is maintained near the start temperature of the transformation. When the temperature goes down to the end temperature of the transformation (which is the start temperature of the following transformation) there is an acceleration of the phase transformation. Thus, since the center is maintained longer to higher temperature, pearlite transformation is slower in this region. Bainite is mainly formed near the internal and external surfaces where cooling is faster. Temperatures near boundaries are rapidly less than the bainite temperature start BS.

Contact pressures evolve along the axial direction. Temperature maps (along radial and axial directions) are presented in figure 12a. The problem being axisymmetric, these maps are sufficient to represent the 3D temperature field. Contact pressures increase from the edges to the coil center (i.e., $Z = 0$). Thus, globally the central zone cools down faster than the edges because of thinner air gaps. However, it should be noticed that internal and external surfaces cool down faster at the edges than near the coil center. Indeed, the air gaps being much larger at the edges, first and last layers are insulated from the hot central core. The insulation due to the air gaps can be observed in figure 12b where the temperature field at $t = 60$ s is depicted at $Z = 0$ mm where contact pressures ensure good conductivity and at $Z = 240$ mm where contact is lost between each layer. (It should be mentioned that Weisz-Patrault et al. [24] modeled a 1500 mm long coil. Here only a 480 mm long sub-part of the coil has been modeled because contact is lost from $Z = \pm 240$ mm to $Z = \pm 750$ mm leading to similar results as for $Z = \pm 240$ mm.)

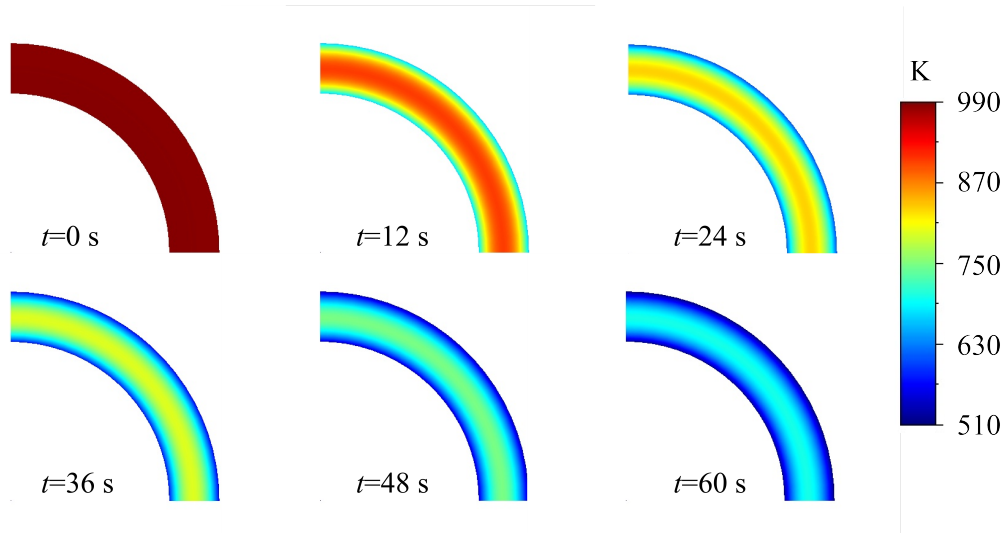
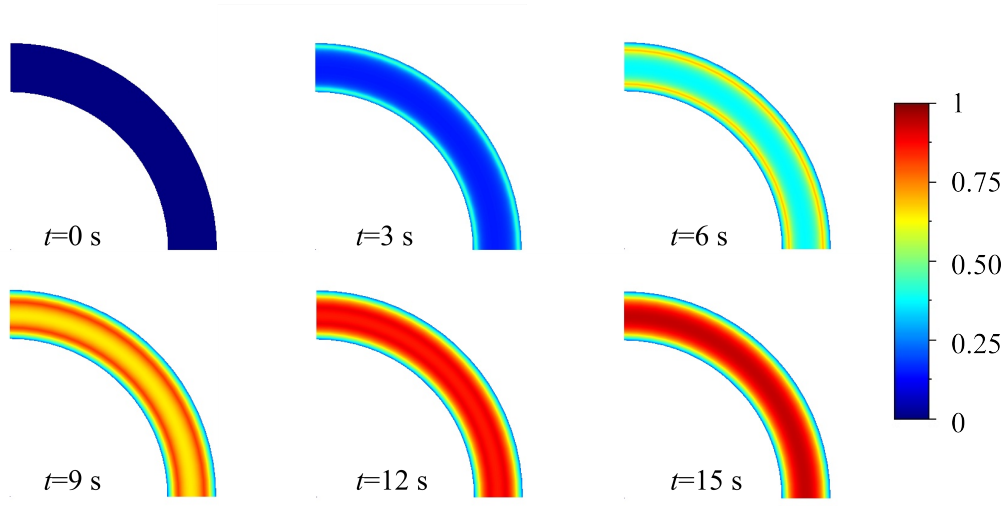
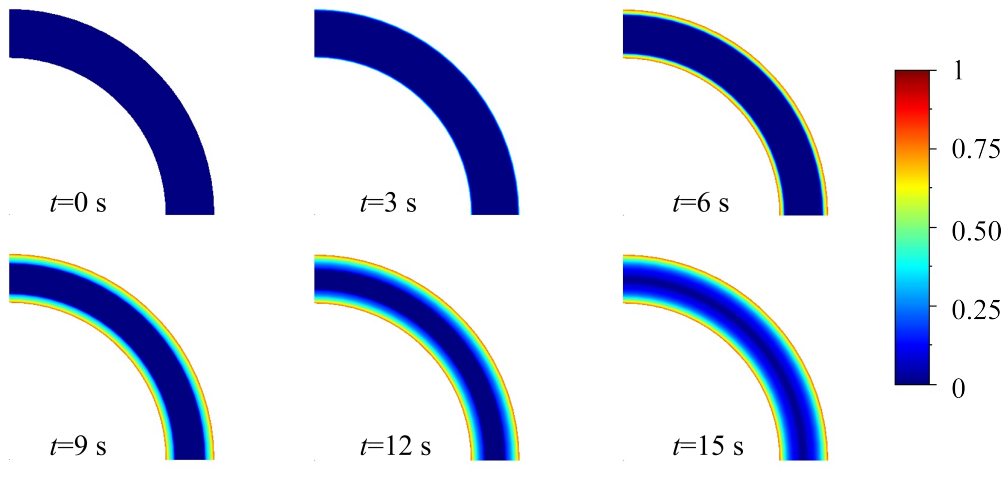


Figure 10: Temperature map at $Z = 0$

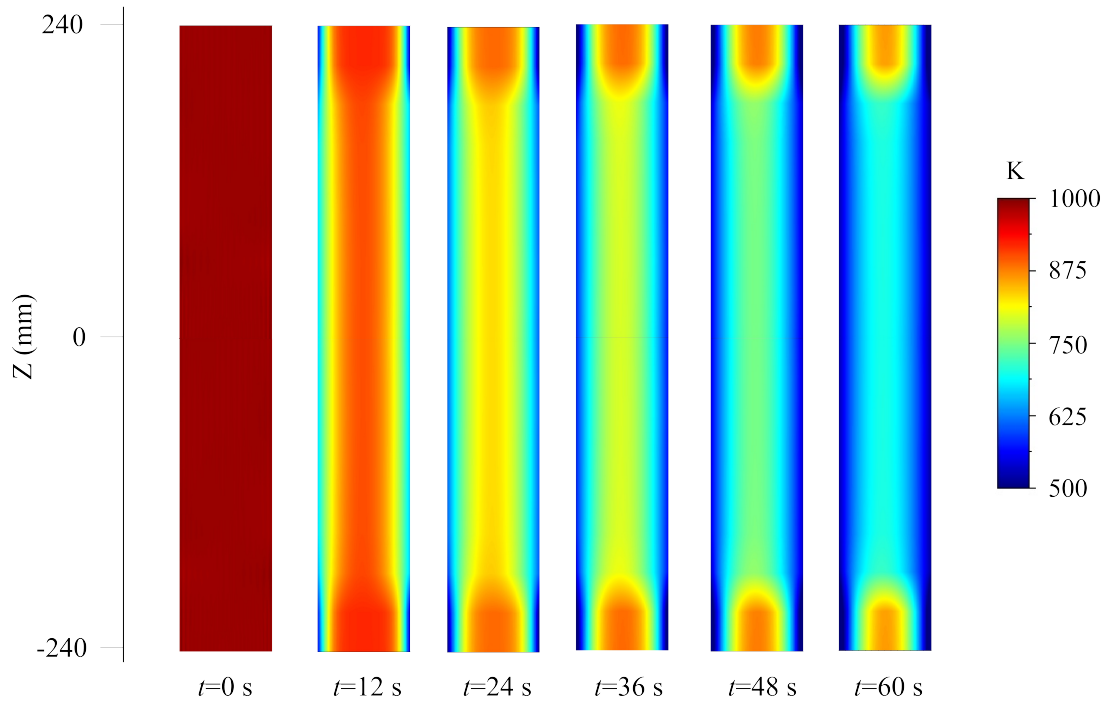


(a) Pearlite phase proportion map at $Z = 0$

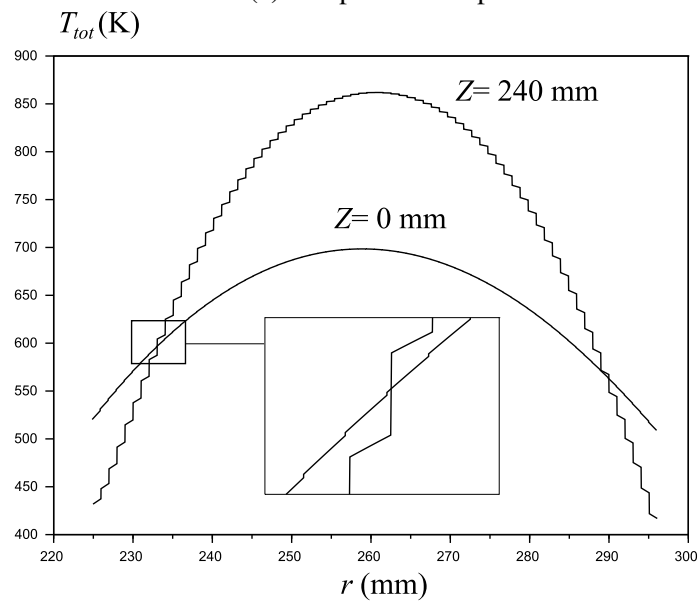


(b) Bainite phase proportion map at $Z = 0$

Figure 11: Phase proportion maps



(a) Temperature maps



(b) Air gap insulation

Figure 12: Temperature field

8. Conclusion

Heat conduction problem coupled with multiphase changes have been solved in a cylindrical multilayer composite accounting for thermal contact resistance depending on contact pressures and roughness. An analytical solution has been proposed, taking into account temperature dependent heat sources. The multiphase change problem is solved using classic Avrami's equation using the isokinetic assumption, in order to deal with non-isothermal conditions. Validation has been carried out using a Finite Element simulation. Outputs consist in temperature and phase fields during cooling. Contact pressure distribution and thermal contact resistance have been taken into account. Significant effects have been found. This coupled problem completes previous works on coiling process and aims at estimating residual stresses. Therefore, subsequent works should develop the mechanical counterpart of the presented model.

Acknowledgment

The author is very grateful to Alain Ehrlicher (Laboratoire Navier, CNRS, École Ponts ParisTech) and to Nicolas Legrand (ArcelorMittal Global Research & Development East Chicago) for their ideas and their help.

Appendix A. Solution for r -dependent right side terms

This appendix presents a particular solution of the following non-homogeneous partial derivative equation:

$$\frac{\partial^2 \widehat{T}^{(i)}}{\partial r^2} + \frac{1}{r} \frac{\partial \widehat{T}^{(i)}}{\partial r} - \frac{1}{D^{(i)}} \frac{\partial \widehat{T}^{(i)}}{\partial t} = \sum_{k=1}^{\widehat{N}_k} \chi_k^{(i)}(r) \exp(-\widehat{\beta}_k^2 t) \quad (\text{A.1})$$

Basis functions, orthogonal with respect to the following scalar product, are needed:

$$\langle g_1, g_2 \rangle_{(i)} = \int_{r^{(i)}}^{r^{(i+1)}} r g_1(r) g_2(r) dr \quad (\text{A.2})$$

Consider the following basis functions:

$$g_l^{(i)} : \begin{cases} [r^{(i)}, r^{(i+1)}] & \rightarrow \mathbb{R} \\ r & \mapsto J_0\left(x_l^{(i)} \frac{r}{r^{(i+1)}}\right) Y_0\left(x_l^{(i)} \frac{r^{(i)}}{r^{(i+1)}}\right) - J_0\left(x_l^{(i)} \frac{r^{(i)}}{r^{(i+1)}}\right) Y_0\left(x_l^{(i)} \frac{r}{r^{(i+1)}}\right) \end{cases} \quad (\text{A.3})$$

where $(x_l^{(i)})_{l \in \{1, \dots, \widehat{N}_l\}}$ are successive roots of $x \mapsto J_0(x) Y_0\left(x \frac{r^{(i)}}{r^{(i+1)}}\right) - J_0\left(x \frac{r^{(i)}}{r^{(i+1)}}\right) Y_0(x)$. Then, it should be noted that $g_l^{(i)}$ vanishes at $r^{(i)}$ and $r^{(i+1)}$. One can prove the following orthogonality properties:

$$\langle g_l^{(i)}, g_m^{(i)} \rangle_{(i)} = \begin{cases} 0 & \text{if } k \neq l \\ M_l^{(i)} > 0 & \text{if } l = m \end{cases} \quad (\text{A.4})$$

Since functions $g_l^{(i)}(r)$ vanish at $r^{(i)}$ and $r^{(i+1)}$ it is convenient to use the orthogonality property (A.4) not directly on $\chi_k^{(i)}(r)$ but on auxiliary functions that vanish at $r^{(i)}$ and $r^{(i+1)}$:

$$\zeta_k^{(i)}(r) = \chi_k^{(i)}(r) - \left(A_k^{(i)} J_0\left(\frac{r}{r^{(i+1)}}\right) + B_k^{(i)} Y_0\left(\frac{r}{r^{(i+1)}}\right) \right) \quad (\text{A.5})$$

where:

$$\begin{pmatrix} A_k^{(i)} \\ B_k^{(i)} \end{pmatrix} = \begin{pmatrix} J_0\left(\frac{r^{(i)}}{r^{(i+1)}}\right) & Y_0\left(\frac{r^{(i)}}{r^{(i+1)}}\right) \\ J_0(1) & Y_0(1) \end{pmatrix}^{-1} \cdot \begin{pmatrix} \chi_k^{(i)}(r^{(i)}) \\ \chi_k^{(i)}(r^{(i+1)}) \end{pmatrix} \quad (\text{A.6})$$

Therefore, using orthogonality properties (A.4), it is obtained:

$$\zeta_k^{(i)}(r) = \sum_{l=1}^{\widehat{N}_l} \zeta_{k,l}^{(i)} g_l^{(i)}(r) \quad (\text{A.7})$$

where:

$$\zeta_{k,l}^{(i)} = \frac{\langle \zeta_k^{(i)}(r), g_l^{(i)}(r) \rangle_{(i)}}{\langle g_l^{(i)}(r), g_l^{(i)}(r) \rangle_{(i)}} \quad (\text{A.8})$$

The right side term of the heat equation (A.1) is written as follows:

$$\sum_{k=1}^{\widehat{N}_k} \chi_k^{(i)}(r) \exp(-\widehat{\beta}_k^2 t) = \sum_{k=1}^{\widehat{N}_k} \left(A_k^{(i)} J_0\left(\frac{r}{r^{(i+1)}}\right) + B_k^{(i)} Y_0\left(\frac{r}{r^{(i+1)}}\right) + \sum_{l=1}^{\widehat{N}_l} \zeta_{k,l}^{(i)} g_l^{(i)}(r) \right) \exp(-\widehat{\beta}_k^2 t) \quad (\text{A.9})$$

Using separation of variables, a particular solution can be written as follows:

$$\widehat{T}^{(i)}(r, t) = \sum_{k=1}^{\widehat{N}_k} \left[\widehat{\Theta}_k^{(i)} J_0\left(\frac{\widehat{\beta}_k}{\sqrt{D^{(i)}}} r\right) + \widehat{\Theta}_k^{(i)} Y_0\left(\frac{\widehat{\beta}_k}{\sqrt{D^{(i)}}} r\right) + \widehat{T}_k^{(i)}(r) \right] \exp(-\widehat{\beta}_k^2 t) \quad (\text{A.10})$$

where:

$$\widehat{T}_k^{(i)}(r) = \sum_{l=1}^{\widehat{N}_l} \left(\frac{\zeta_{k,l}^{(i)}}{\frac{\widehat{\beta}_k}{\sqrt{D^{(i)}}} - \left(\frac{x_l^{(i)}}{r^{(i+1)}}\right)^2} \right) g_l^{(i)}(r) + \frac{A_k^{(i)} J_0\left(\frac{r}{r^{(i+1)}}\right) + B_k^{(i)} Y_0\left(\frac{r}{r^{(i+1)}}\right)}{\frac{\widehat{\beta}_k}{\sqrt{D^{(i)}}} - \left(\frac{1}{r^{(i+1)}}\right)^2} \quad (\text{A.11})$$

References

- [1] F. De Monte, Transient heat conduction in one-dimensional composite slab. a natural analytic approach, *International Journal of Heat and Mass Transfer* 43 (2000) 3607–3619.
- [2] F. De Monte, An analytic approach to the unsteady heat conduction processes in one-dimensional composite media, *International Journal of Heat and Mass Transfer* 45 (2002) 1333–1343.
- [3] F. De Monte, Unsteady heat conduction in two-dimensional two slab-shaped regions. exact closed-form solution and results, *International Journal of Heat and Mass Transfer* 46 (2003) 1455–1469.
- [4] S. Singh, P. K. Jain, et al., Analytical solution to transient heat conduction in polar coordinates with multiple layers in radial direction, *International Journal of Thermal Sciences* 47 (2008) 261–273.
- [5] P. K. Jain, S. Singh, et al., Analytical solution to transient asymmetric heat conduction in a multilayer annulus, *Journal of Heat Transfer* 131 (2009) 011304.

- [6] P. K. Jain, S. Singh, et al., An exact analytical solution for two-dimensional, unsteady, multilayer heat conduction in spherical coordinates, *International Journal of Heat and Mass Transfer* 53 (2010) 2133–2142.
- [7] M. Li, A. C. Lai, Analytical solution to heat conduction in finite hollow composite cylinders with a general boundary condition, *International Journal of Heat and Mass Transfer* 60 (2013) 549–556.
- [8] M. Necati Özışık, *Boundary value problems of heat conduction*, Dover, 1968. 3rd edition (2002).
- [9] G. Kaza, Contribution à l'étude de la résistance thermique de contact et à sa modélisation à travers l'écrasement de l'interface tôle/outil dans la mise en forme à chaud de tôles d'acier, Ph.D. thesis, Université de Toulouse, Université Toulouse III-Paul Sabatier, 2010.
- [10] Y. P. Shlykov, Y. A. Ganin, Thermal resistance of metallic contacts, *International Journal of Heat and Mass Transfer* 7 (1964) 921–929.
- [11] M. Cooper, B. Mikic, M. Yovanovich, Thermal contact conductance, *International Journal of Heat and Mass Transfer* 12 (1969) 279–300.
- [12] B. Mikić, Thermal constriction resistance due to non-uniform surface conditions; contact resistance at non-uniform interface pressure, *International Journal of Heat and Mass Transfer* 13 (1970) 1497–1500.
- [13] B. Mikić, Thermal contact conductance; theoretical considerations, *International Journal of Heat and Mass Transfer* 17 (1974) 205–214.
- [14] A. Hamasaiid, M. Dargusch, T. Loulou, G. Dour, A predictive model for the thermal contact resistance at liquid–solid interfaces: analytical developments and validation, *International Journal of Thermal Sciences* 50 (2011) 1445–1459.
- [15] C. Yuan, B. Duan, L. Li, B. Shang, X. Luo, An improved model for predicting thermal contact resistance at liquid–solid interface, *International Journal of Heat and Mass Transfer* 80 (2015) 398–406.
- [16] C. Fieberg, R. Kneer, Determination of thermal contact resistance from transient temperature measurements, *International Journal of Heat and Mass Transfer* 51 (2008) 1017–1023.
- [17] Y.-T. Pan, Measurement and Modelling of Diffusional Transformation of Austenite in C-Mn Steels, Ph.D. thesis, National Sun Yat-Sen University, 2001.
- [18] M. Avrami, Kinetics of phase change. i general theory, *The Journal of Chemical Physics* 7 (1939) 1103–1112.
- [19] J. W. Cahn, The kinetics of grain boundary nucleated reactions, *Acta Metallurgica* 4 (1956) 449–459.
- [20] J. W. Christian, *The Theory of Transformations in Metals and Alloys*, Pergamon, 1965. 3rd edition (2002).

- [21] D. Koistinen, R. Marburger, A general equation prescribing the extent of the austenite-martensite transformation in pure iron-carbon alloys and plain carbon steels, *acta metallurgica* 7 (1959) 59–60.
- [22] D. Weisz-Patrault, A. Ehrlacher, N. Legrand, E. Mathey, Non-linear numerical simulation of coiling by elastic finite strain model, *Key Engineering Materials* 651-653 (2015) 1060–1065.
- [23] D. Weisz-Patrault, A. Ehrlacher, Curvature of an elasto-plastic strip at finite strains: application to fast simulation of coils, in: 22ième Congrès Français de Mécanique, AFM, Association Française de Mécanique, pp. 1–14.
- [24] D. Weisz-Patrault, A. Ehrlacher, N. Legrand, Non-linear simulation of coiling accounting for roughness of contacts and multiplicative elastic-plastic behavior, *International Journal of Solids and Structures* 94-95 (2016) 1–20.
- [25] S.-J. Park, B.-H. Hong, S. C. Baik, K. H. Oh, Finite element analysis of hot rolled coil cooling., *ISIJ International* 38 (1998) 1262–1269.
- [26] A. Saboonchi, S. Hassanpour, Heat transfer analysis of hot-rolled coils in multi-stack storing, *Journal of Materials Processing Technology* 182 (2007) 101–106.
- [27] M. Karlberg, Modelling of the temperature distribution of coiled hot strip products, *ISIJ International* 51 (2011) 416–422.
- [28] R. Mehta, S. S. Sahay, Heat transfer mechanisms and furnace productivity during coil annealing: aluminum vs. steel, *Journal of Materials Engineering and Performance* 18 (2009) 8–15.
- [29] M.-G. Lee, S.-J. Kim, H. N. Han, W. C. Jeong, Implicit finite element formulations for multi-phase transformation in high carbon steel, *International Journal of Plasticity* 25 (2009) 1726–1758.
- [30] E. Hawbolt, B. Chau, J. Brimacombe, Kinetics of austenite-ferrite and austenite-pearlite transformations in a 1025 carbon steel, *Metallurgical Transactions A* 16 (1985) 565–578.
- [31] H. N. Han, J. K. Lee, H. J. Kim, Y.-S. Jin, A model for deformation, temperature and phase transformation behavior of steels on run-out table in hot strip mill, *Journal of Materials Processing Technology* 128 (2002) 216–225.